Journal of Geochemical Exploration 183 (2017) 79–87

Contents lists available at ScienceDirect

Journal of Geochemical Exploration

journal homepage: www.elsevier.com/locate/gexplo

Occurrence, source and enrichment mechanism of silver in black shale-hosted Baiguoyuan Ag-V ore deposit, Hubei Province, China

Yan Yi[a], Dao-Hui Pi[a,*], Shao-Yong Jiang[a,b,*]

[a] State Key Laboratory of Geological Processes and Mineral Resources, Collaborative Innovation Center for Exploration of Strategic Mineral Resources, Faculty of Earth Resources, China University of Geosciences, Wuhan 430074, China

[b] State Key Laboratory for Mineral Deposits Research, Department of Earth Sciences, Nanjing University, Nanjing 210093, China

ARTICLE INFO

Keywords:
Occurrence of silver
Mineral chemistry
Pyrite
Naumannite
Baiguoyuan Ag-V ore deposit

ABSTRACT

The Baiguoyuan Ag-V ore deposit in Xingshan County, Hubei Province, is hosted in Neoproterozoic black shale, containing approximately 1860 tons Ag at average grade of 116 g/t and 21.8 Mt. V at average grade of 1.5%. The occurrence, source and enrichment mechanism of silver in this deposit are still a topic of debate. In this study, we applied high-resolution electron microprobe analysis (EMPA) and LA-ICP-MS technique to determine the occurrence of silver and to infer its source and enrichment mechanism. Mineralography observation revealed that pyrite is the main metallic mineral in the ores, which shows three-stage formation histories: (1) sedimentation, (2) diagenesis, and (3) deformation. BSE imaging detected tiny naumannite inclusions in pyrite. EMPA showed high contents of Ag in sedimentary pyrite. LA-ICP-MS analysis displayed both solid solution and tiny naumannite inclusion of Ag in pyrite. A mass balance calculation suggested that Ag occurred mainly as solid solution and minor as tiny naumannite inclusions in pyrite. The high contents of Co and Se, and high ratios of Co/Ni and Se/S in sedimentary pyrite indicated that Ag was probably supplied by submarine hydrothermal venting. The correlation between Ag and Fe or Se in sedimentary pyrite indicated that Ag was enriched through Ag and Se replacing Fe and S in pyrite, respectively.

1. Introduction

The occurrence of silver in many ore deposits is significant for understanding its mineralization and utilization (Cabri, 1992; Sharp and Buseck, 1993; Costagliola et al., 2003). In volcanic epithermal ore deposits, Ag mainly occurs as Ag sulfides (andorite, polybasite and pyrargyrite), electrum, and naumannite, and minor enters into the lattice of galena and pyrite (Kamenov et al., 2007; Deditius et al., 2011; Cocker et al., 2013; Zhuravkova et al., 2015; Tian, 2015). In volcanic-hosted massive sulfide (VMS) and sedimentary-exhalative (SEDEX) Ag-Pb-Zn ore deposits, Ag enters into the lattice of galena, chalcopyrite, tennantite and tetrahedrite (Huston et al., 1995; Kelly et al., 2004; Gadd et al., 2016).

The Baiguoyuan Ag-V ore deposit in Xingshan County, Hubei Province, is hosted in the Neoproterozoic black shales. It contains approximately 1863 tons Ag at average grade of 116 g/t and 21.8 Mt. V at average grade of 1.5% (Li et al., 2014). The ore deposit geology indicated that it could be a new type of Ag ore deposit (Chen and Xie, 1986; Hua, 1988; Zhang et al., 1995; Yang et al., 1996; Chen et al., 1997; Zhuang et al., 1999; Yang et al., 2011). The Ag occurrence in the Baiguoyuan deposit has been investigated by a number of researchers, but its metallogenesis is still debatable. The main reason is that those previous works were carried out with conventional methods of microscopy observation, wet chemical analysis, and low resolution electron microprobe analysis (EMPA), which led to great uncertainty in distinguishing Ag occurrence (Chen and Xie, 1986; Zhang et al., 1995; Liu et al., 1996; Chen et al., 1997; Zhuang et al., 1999; Lu et al., 1999). In this study, we used high-resolution EMPA and LA-ICP-MS methods, to reveal the Ag occurrence in the Baiguoyuan Ag-V ore deposit, and to constrain its source and enrichment mechanism.

2. Geological setting

2.1. Regional geology

During the Neoproterozoic Ediacaran stage (635–541 Ma), a platform was inferred to develop over a rifted continental margin at the southeastern side of the Yangtze Block (Jiang et al., 2011). During deposition of the Doushantuo Formation (635–551 Ma) and Dengying Formation (551–541 Ma), four sedimentary facies are distinguished:

* Corresponding authors at: State Key Laboratory of Geological Processes and Mineral Resources, Collaborative Innovation Center for Exploration of Strategic Mineral Resources, Faculty of Earth Resources, China University of Geosciences, Wuhan 430074, China.
E-mail addresses: 1415662446@qq.com (Y. Yi), daohuipi@cug.edu.cn (D.-H. Pi), shyjiang@cug.edu.cn (S.-Y. Jiang).

http://dx.doi.org/10.1016/j.gexplo.2017.10.005
Received 1 November 2016; Received in revised form 17 September 2017; Accepted 3 October 2017
Available online 04 October 2017
0375-6742/

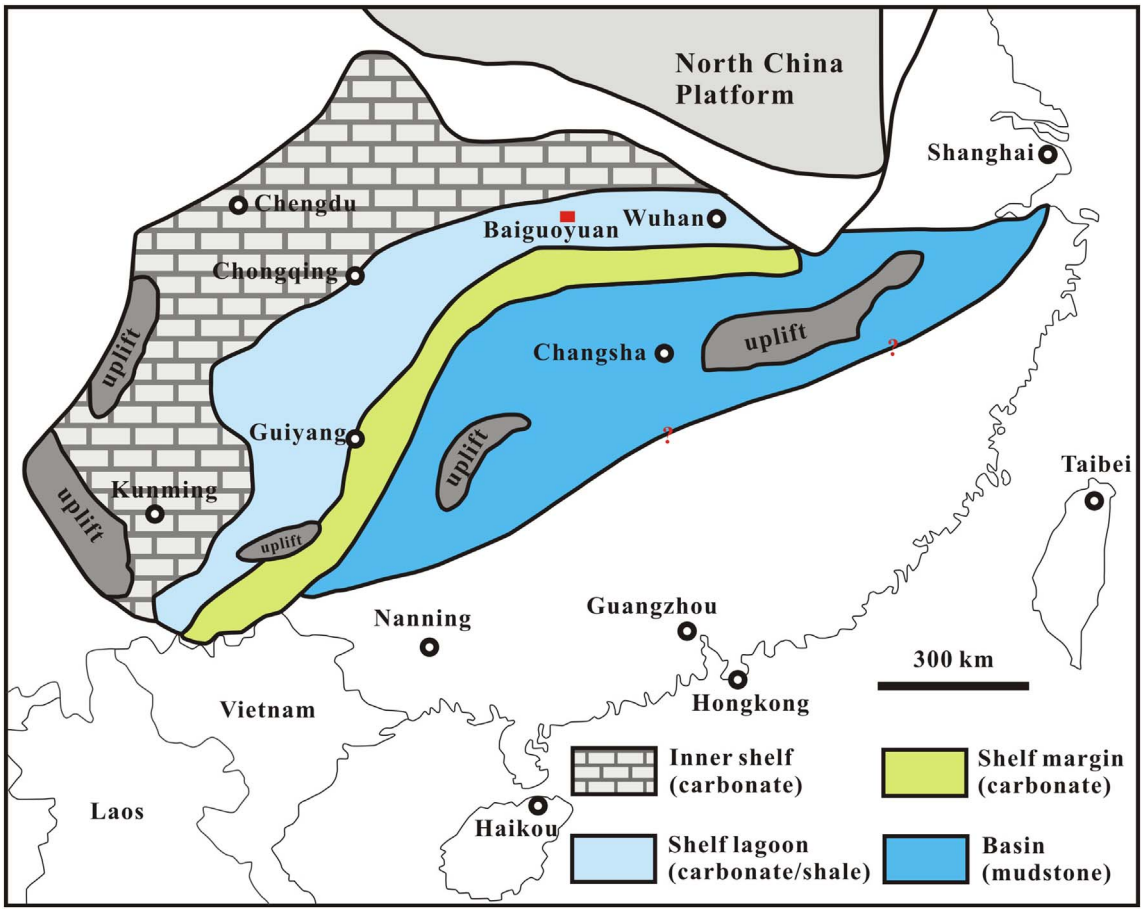

Fig. 1. Paleogeography of the Yangtze Platform during deposition of the Neoproterozoic Ediacaran Doushantuo Formation (after Jiang et al., 2011).

inner shelf, shelf lagoon, shelf margin and basin from northwestern to southeastern (Fig. 1). The Doushantuo Formation strata vary in thickness from 90 m in the inner shelf to 200 m in the basin. It is mainly composed of carbonate rock, but in the shelf lagoon facies, at the top of Doushantuo Formation occurred organic-rich black shales which hosted the Baiguoyuan Ag-V ore deposit (Jiang et al., 2011).

2.2. Ore deposit geology

The Baiguoyuan Ag-V ore deposit is located about 33 km northeast of Xingshan County, Hubei Province, China. Strata exposed in the mining area, from youngest to oldest age include (Fig. 2 and Fig. 3A): (1) Shuijingtuo Formation of lower Cambrian, composed mainly of silty limestone and silty dolomite; (2) Dengying Formation of Neoproterozoic Ediacaran, composed mainly of muddy dolomite and micritic dolomite; (3) Doushantuo Formation of Neoproterozoic Ediacaran, composed of interbedded muddy dolomite, black shale, silty dolomite, phosphate rock and siliceous rock; (4) Nantuo Formation of Neoproterozoic Cryogenian, composed of glacial diamictite; and (5) Huanglianghe Formation of Paleoproterozoic Shuiyuesi Group, composed of migmatite, biotitic plagioclase gneiss, hornblende schist and chlorite schist. The large NW striking Zhangshuping fault crosscuts all the sedimentary strata in the southwestern part (Fig. 2), while several small-scale faults of NW, NNW and NE striking developed only within the Neoproterozoic strata (Fig. 2).

The ore-hosted Ediacaran Doushantuo Formation consists of four members in the mining area (Fig. 3A).

Member 1 (Pt_3d^1): light grey thick dolomite with great variation in thickness from 0 to 3 m (average 2.0 m). This strata is called as cap carbonate in the Three Gorges area (Zhu et al., 2013b).

Member 2 (Pt_3d^2): phosphorus-bearing dolomite in the lower part, grey thin-bedded muddy dolomite intercalated with dolomitic mudstone in the middle part and light grey thick-bedded dolomite intercalated with fine-laminated dolomite in the upper part. This unit is 15.7 to 63.0 m (average 41.8 m) in thickness.

Member 3 (Pt_3d^3): dark grey muddy dolomite intercalated with black banded or nodular chert. Thickness varies greatly between 31.0 m and 77.5 m (average 38.8 m).

Member 4 (Pt_3d^4): black grey thick-bedded muddy dolomite interbedded with black shale in the lower part, and black shale interbedded with minor dolomite in the upper part (Fig. 3B). The thickness of this unit is ca. 8.2 to 16.8 m (average13.5 m).

The stratiform ore body is hosted in the Member 4 of the Doushantuo Formation (Fig. 3B, C). It can be divided into two ore layers: The lower ore layer is hosted in the lower part of Member 4, which is the main Ag-V ore layer with about 2 m to 6 m thick and average grade of 1% to 1.25% V_2O_5 and 10 to 299 ppm Ag (Fig. 3B). The upper ore layer is hosted in the upper part of Member 4, about 1 m to 3 m thick and has V_2O_5 of 0.5% to 0.7% and Ag of ca. 70 ppm (Fig. 3B).

The metallic minerals in ores are mainly pyrite, and few naumannite has also been detected in this study (Fig. 4). Previous literatures reported occurrence of minor chalcopyrite and marcasite, (Chen and Xie, 1986; Liu et al., 1996), but we did not observed these minerals in this study. The nonmetallic minerals in ores are mainly illite and dolomite, with some amounts of barite and minor quartz and apatite. The ores show banding, lamellar (Fig. 3D) and nodular structures and typical lamination texture.

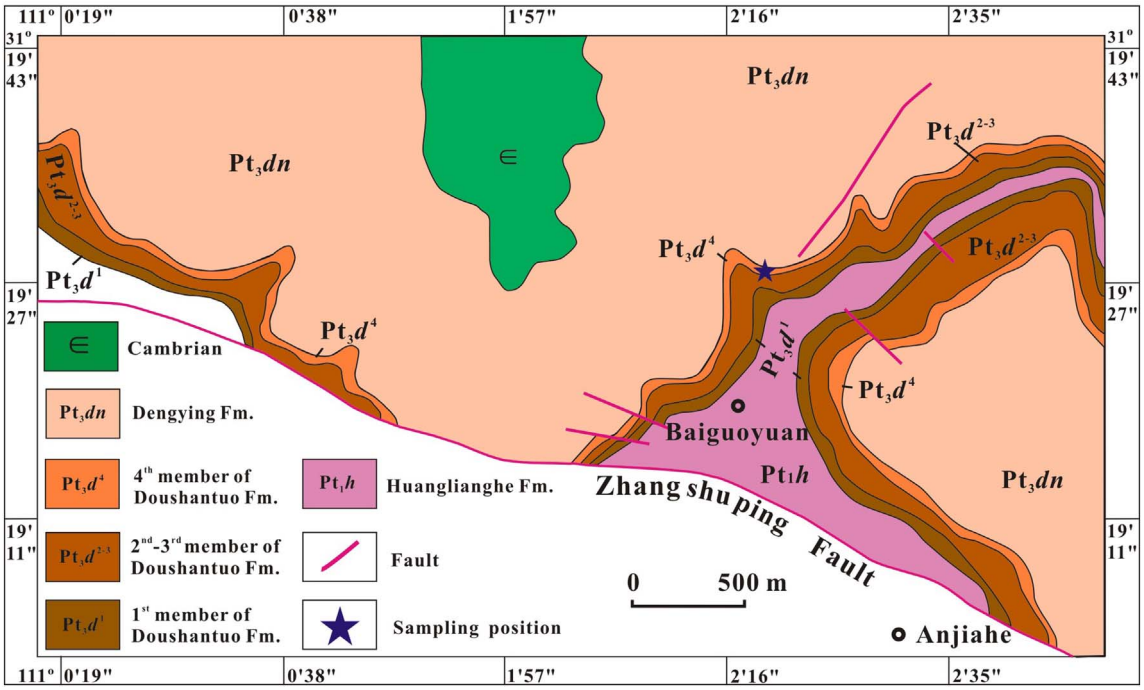

Fig. 2. Geological sketch map of the Baiguoyuan Ag-V ore deposit, Hubei Province (after Yang et al., 2011).

3. Sampling and analytical methods

In this study, a total of 43 samples were collected from the lower ore layer and were made into polished sections for reflected light microscopy study. Among them, 14 samples were further selected for pyrite chemical composition study by high-resolution EMPA and LA-ICP-MS techniques.

The EMPA analyses were carried out at the State Key Laboratory of Geological Processes and Mineral Resources, China University of Geosciences (Wuhan), with a JEOL JXA-8100 Electron Probe Micro Analyzer equipped with four wavelength-dispersive spectrometers (WDS). The samples were firstly coated with a thin conductive carbon film prior to analysis. The precautions suggested by Zhang and Yang (2016) were used to minimize the difference of carbon film thickness between samples and obtain a ca. 20 nm approximately uniform coating. During the analysis, we used backscattered electron images to help selection of analytical points and identify unknown minerals. Pyrites in this study were analyzed for Fe, S, Co, Ni, Ag, Se, Cu, Pb, Zn, Ge, Ti and V. Standards used for each element were natural pyrite (for Fe and S), Cobalt, Nickel, Silver, Selenium, Copper, Galena, Zinc, Germanium, Titanium and Vanadium. An accelerating voltage of 20 kV, a beam current of 20 nA and a 2 μm spot beam were used. Data were corrected on-line using a modified ZAF (atomic number, absorption, fluorescence) correction procedure. Element peaks and backgrounds were measured for all elements with counting times of 10 s and 5 s. The average detection limits for pyrite were Fe (135 ppm), S (172 ppm), Co (124 ppm), Ni (115 ppm), Ag (133 ppm), Se (98 ppm), Cu (107 ppm), Pb (169 ppm), Zn (100 ppm), Ge (113 ppm), Ti (88 ppm) and V (174 ppm). We only report analyses whose analytical totals were within the range from 98 to 102 wt%.

The LA-ICP-MS analyses were conducted at Nanjing FocuMS Technology Company Limited. Photon Machines Excite 193 laser microprobe (Teledyne Cetac Technologies) is coupled to an Agilent 7700 × quadrupole mass-spectrometer. Ablation was conducted with a laser pulse rate of 6 to 8 Hz using beam fluences at 6 to 7 J/cm^2, beam size of 25 to 50 μm and carrier gas of pure He. A background analysis of 15 s was measured prior to a 40 s period of laser ablation for each analysis. Calibration standards NMC-12744 and USGS GSE-1G were analyzed once between every 10 unknown sample analyses.

4. Results

4.1. Pyrite texture and composition

Pyrite is the dominant sulfide mineral in the Baiguoyuan Ag-V ore deposit, and accounts for ~5% to ~15% in the ores. Microscopy observation, back scattered electron imaging (BSE) and EMPA revealed that individual pyrite shows great varieties in shape, size, internal texture, and chemical composition (Fig. 4; Table 1). According to the occurrence of pyrite in the ores, four pyrite types can be distinguished, namely framboid pyrite (Py1), lamina pyrite (Py2), rim pyrite (Py3), and vein pyrite (Py4).

Framboid pyrite (Py1) consists of spherical aggregates of microcrystalline (< 1 μm) and usually disseminated in the muddy dolomite. Individual framboid is generally < 10 to 20 μm in diameter (Fig. 4A). This occurrence of pyrite is rare, and < 0.1% in the ores. Because of the small size of individual pyrite, they were not measured for chemical compositions by EMPA.

Lamina pyrite (Py2) consists of subhedral to euhedral pyrite crystals, which aggregate as laminae from < 1 mm to several millimeters thick. They can be divided into 2 subtypes. One is coarse-grained, euhedral, inclusion-free pyrite (Py2a), which is generally 100 to 300 μm in size and formed discontinuous laminae in dolomites (Fig. 4B, C). Locally, Py2a is overgrown by late anhedral pyrite (Py2b) (Fig. 4D). This occurrence of pyrite is quite few, and accounts for ca. 1% in the ores. Py2a is characterized by the lowest contents of Fe (44.6–46.1% with a mean value of 45.5%) and S (52.4–54.4% with a mean value of 53.3%) and the highest contents of Ag (up to 6360 ppm, a mean value of 2712 ppm) and Se (up to 3210 ppm, a mean value of 1707 ppm). The Ag content displays a negative correlation with Fe, and a positive correlation with Se (Fig. 5). The concentrations of Co are relative low (380–970 ppm with a mean value of 733 ppm). The Co/Ni ratios vary from below 1 to over 5 with most higher than 1 (Fig. 5).

The second subtype of Lamina pyrite (Py2) is fine-grained (< 50 μm) euhedral inclusion-rich pyrite (Py2b), which formed continuous laminae in the muddy dolomite (Fig. 4E). This occurrence of

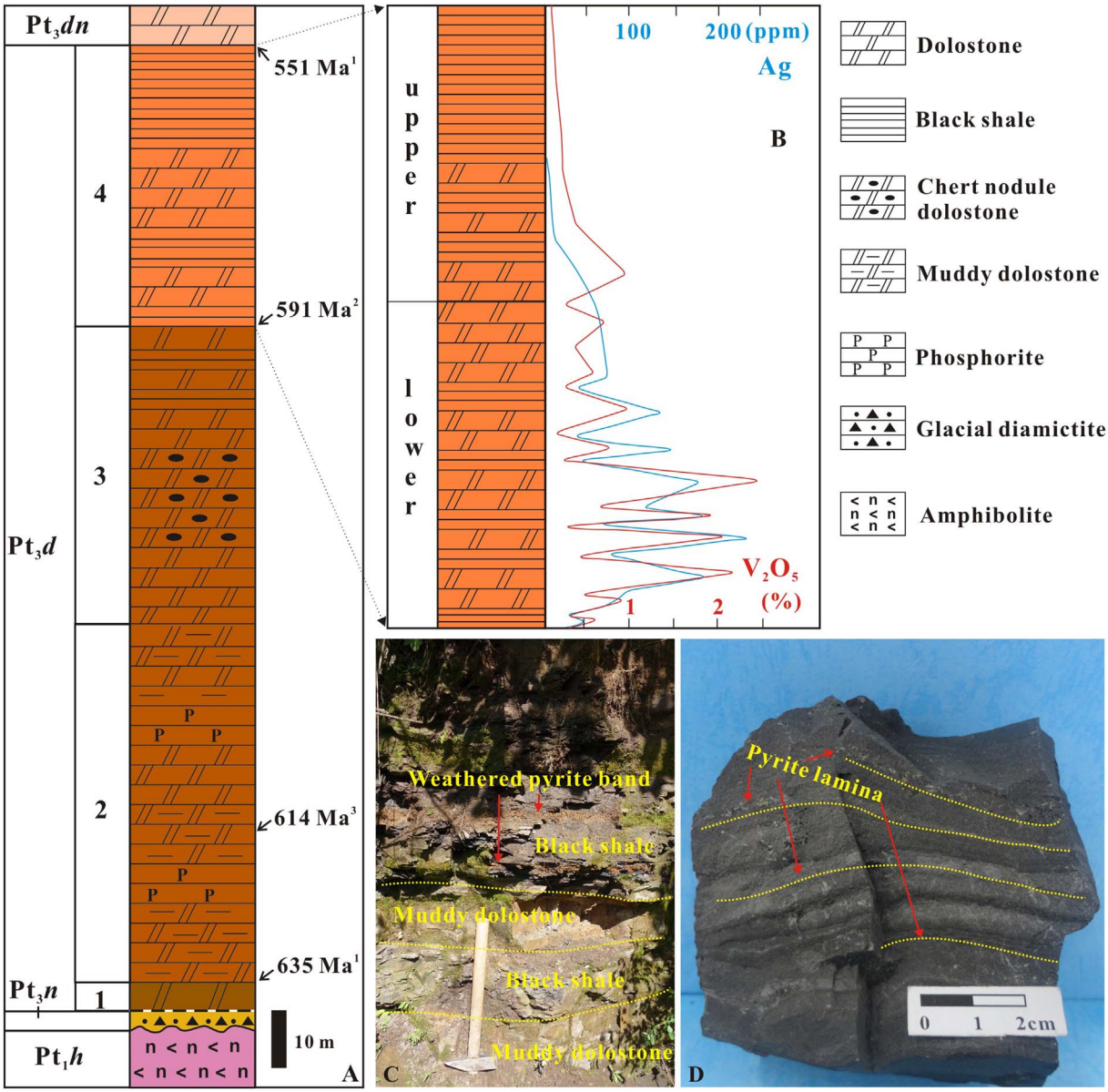

Fig. 3. Stratigraphic column and field photos of the Baiguoyuan Ag-V ore deposit, Hubei Province. A) Stratigraphic column in the Baiguoyuan area (modified after Zhu et al., 2013a, b); B) Stratigraphic variation of Ag and V_2O_5 content (plotted according to data from Chen and Xie,1986); C) Photo of the lower stratiform ore body; D) Photo of ore with lamellar structure. Age data: [1] from Condon et al. (2005), [2] from Zhu et al. (2013a, b), and [3] from Liu et al. (2009).

pyrite is ubiquitous, and accounts for ca. 10% in the ores. Py2b shows relative high contents of Fe (44.4–46.9% with a mean value of 45.8%), S (52.4–55.2% with a mean value of 53.7%) and Co (460–1140 ppm with a mean value of 761 ppm), in contrast their contents of Ag (up to 3470 ppm with a mean value of 429 ppm) and Se (up to 4380 ppm with a mean value of 491 ppm) are relatively lower than the Py1 and Py2a. No obvious correlations are observed between the Ag contents and the Fe and Se contents (Fig. 5). The Co/Ni ratios vary from below 1 to over 7 with most higher than 1 (Fig. 5).

Rim pyrite (Py3) refers to the pyrite overgrowth around coarse-grained barite (Fig. 4F) and pyrite (Fig. 4D). This occurrence of pyrite is substantial, and accounts for ca. 5% in the ores. Py3 shows moderate concentrations of Fe (44.9–46.9% with a mean value of 45.9%) and S (52.4–54.8% with a mean value of 53.4%). The concentration of Co (480–1040 ppm with a mean value of 759 ppm) is close to that of Py2b. The concentrations of Ag (a mean value of 270 ppm) and Se (a mean value of 310 ppm) are relatively lower than Py1 and Py2. No correlations are observed between the Ag contents and the Fe and Se contents (Fig. 5). The Co/Ni ratios are all higher than 1 (Fig. 5).

Vein pyrite (Py4) represents pyrite vein (about 0.5 cm long) that crosscuts the muddy dolomite laminae (Fig. 4G). The vein mainly consists of pyrite with minor amount of barite, dolomite and clay minerals. This occurrence of pyrite is very rare, and < 0.1% in the ores. Py4 is characterized by the highest concentrations of Fe (46.0–47.1% with a mean value of 46.3%) and S (63.0–53.9% with a mean value of 53.5%). The contents of Se and Ag are the lowest with most below detection limits, while the concentrations of Co (710–1110 ppm with a mean value of 903 ppm) are the highest. No correlations are present between the Ag contents and the Fe and Se contents (Fig. 5). The Co/Ni ratios are all higher than 2 (Fig. 5).

4.2. Other minerals and their compositions

Dolomite is the main nonsulfide mineral in the Baiguoyuan Ag-V ore deposit, and accounts for ~85% to ~95% in the ores (Fig. 6A). Microscopy observation and BSE imaging revealed that individual

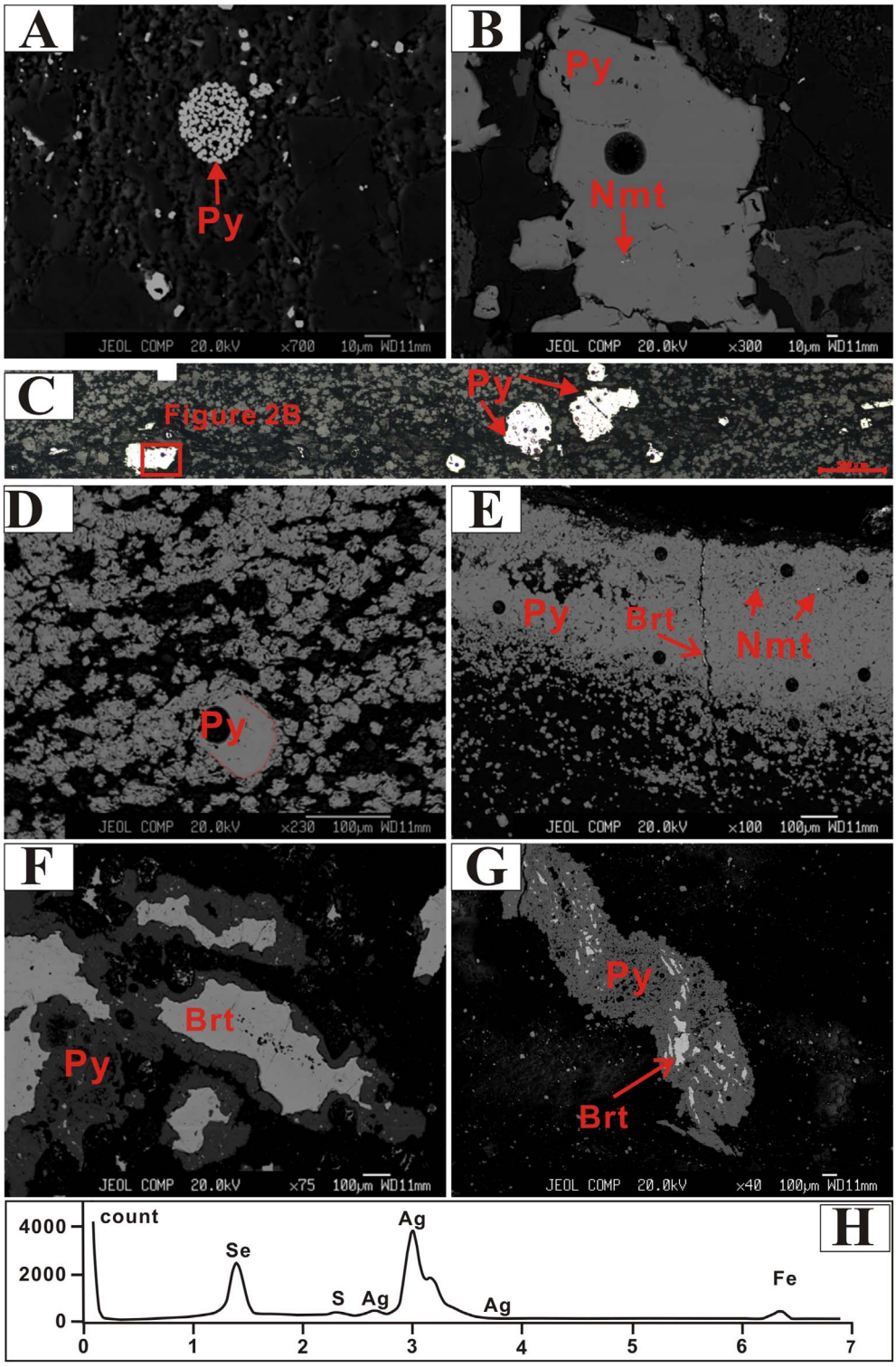

Fig. 4. BSE images and reflected light photographs of different occurrences of pyrite from the Baiguoyuan Ag-V ore deposit, Hubei Province. A) Framboidal pyrite (Py1). B) Coarse-grained euhedral pyrite (Py2a). Naumannite (white spots) occurs as micron inclusions in pyrite. C) Py2a occurs as discontinuous laminae. D) Py2a is overgrown by late anhedral pyrite (Py3). E) Fine-grained pyrite (Py2b) makes up of laminae that preserve primary bedding of the host muddy dolomite. Naumannite (white spots) occurs as micron inclusions in pyrite. F) Rim pyrite (Py3) occurs as rim of euhedral barite. G) Vein pyrite (Py4) crosscuts the muddy dolomite laminae. H) EDS spectra of naumannite.
Py = pyrite, Nmt = Naumannite, Brt = barite, Dol = dolomite, Ap = apatite.

dolomite crystal is subhedral to euhedral with grain size varying from < 10 μm to > 100 μm (Fig. 6B). They arranged as laminae interbedded by pyrite and barite laminae (Fig. 6A). In many cases, they are present in the pyrite laminae with varying proportions.

Illite occurs but is very few, and accounts for ~1% in the ores. BSE imaging revealed that individual illite is very small in size less than < 3 μm (Fig. 6B). Illite dispersed in the dolomite, and sometimes included within pyrite as revealed by LA-ICP-MS spectrum (Fig. 6D). Previous study reported that the illite could account for 50% of the clay minerals in the ores, and is the main carrier of V (Chen and Xie, 1986).

Barite accounts for ~5% in the ores (Fig. 6A). Barite commonly shows euhedral prism up to several millimeters long, and occurs as thin laminae in the dolomite. On the rim of barite overgrows Py3 (Fig. 6C).

Apatite and quartz are also found in the ores. Apatite is present in the muddy dolomite laminae (Fig. 6B), while quartz occurred with barite (Fig. 6C).

In addition, tiny Ag mineral was detected in this study. The Ag mineral is likely naumannite based on EDS spectra (Fig. 4H). The grain is too small, ranging from 1 μm to 2 μm in size, to perform quantitative analysis. This Ag mineral occurs as inclusions in Py2a and Py2b

Table 1
Statistic of chemical compositions of pyrite from the Baiguoyuan Ag-V ore deposit, Hubei Province.

Pyrite type	Py2a (n = 28)	Py2b (n = 87)	Py3 (n = 39)	Py4 (n = 7)
S (%)	52.4–54.4	52.4–55.2	52.4–54.8	53.0–53.9
	53.3	53.6	53.4	53.5
Fe (%)	44.6–46.1	44.4–46.9	44.9–46.9	46.0–47.1
	45.5	45.8	45.9	46.3
S + Fe (%)	97.5–99.9	97.9–101.6	98.0–101.6	99.3–100.9
	98.8	99.5	99.3	99.9
Se (ppm)	420–3210	110–4380	100–1650	170–580
	1771	785	553	305
Ag (ppm)	560–6360	140–3470	140–5150	320
	3157	805	673	320
Co (ppm)	380–970	460–1140	480–1040	710–1110
	733	761	759	903
Ni (ppm)	150–1390	120–3090	120–440	260–450
	403	360	220	330
Co/Ni	0.47–5.50	0.33–9.00	1.52–5.59	2.31–4.27
	2.62	3.8	3.90	2.98
S/Se	166–1284	123–4933	328–5333	925–3162
	437	1631	1775	2210

(Fig. 4B, E), which was also confirmed by the LA-ICP-MS spectrum (Fig. 6E). It is noted that As and V are both redox sensitive elements and behave similarly, however, As contents in pyrite are low as indicated by the LA-ICP-MS spectrum (Fig. 6E, F).

5. Discussion

5.1. Origin of pyrite

The two earliest forms of pyrite (Py2a and Py2b) commonly occurred as laminae of coarse-grained euhedral, and fine-grained inclusion-rich subhedral crystals, which are interpreted as synsedimentary to early diagenetic in origin. The fine grained framboid pyrite (Py1) occurs as dissemination within the dolomite and is interpreted to form during early to late diagenesis. The pyrite overgrowth (Py3) on the earlier pyrite and barite is interpreted to form during late diagenesis. The late stage, inclusion-rich pyrite (Py4) crosscuts the dolomite and is considered to form during early deformation stage.

Compared with the compositions of Neoproterozoic sedimentary pyrite compiled by Gregory et al. (2015), our pyrite samples show relative higher Ag, Se and Co contents, and lower Ni contents. The increase in Ag, Se and Co may be related to submarine hydrothermal activity which supply enough trace elements for pyrite incorporation. The decrease in Ni may be related to low content of organic matter which supply less Ni for pyrite incorporation during the decay of organic matter.

5.2. Occurrence of Ag

The Ag has two occurrences as revealed in this study. One is micron-grained naumannite, and the other is invisible Ag in pyrite. The latter occurrence as solid solution in pyrite is the main carrier of Ag.

Naumannite is closely related to pyrite laminae, occurring as tiny inclusion (< 2 μm) in Py2a and Py2b (Fig. 4B, E). It is the only Ag mineral found in this study, but previous works reported presence of Ag minerals such as native silver, argentite, acanthite, and aguilarite in the

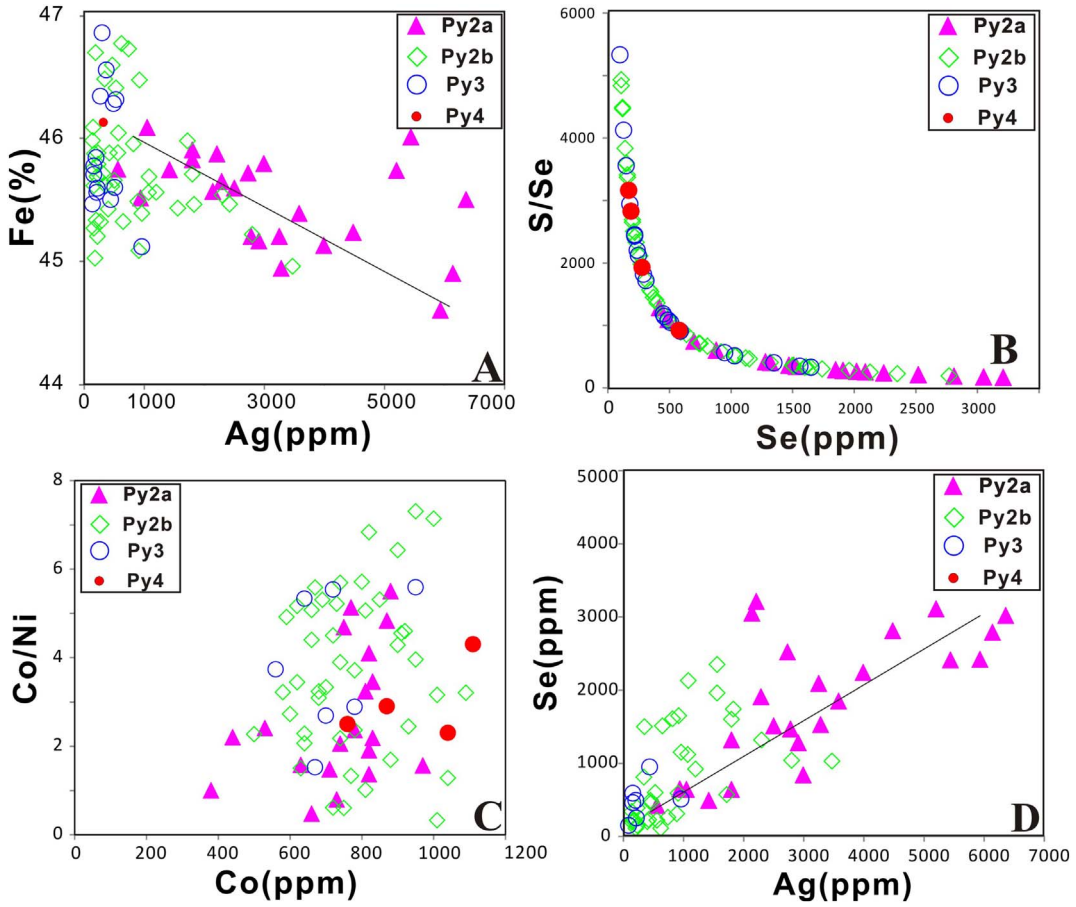

Fig. 5. Plots of chemical compositions of pyrite from the Baiguoyuan Ag-V ore deposit, Hubei Province. A) Ag vs. Fe, B) Se vs. S/Se, C) Co vs. Co/Ni, D) Ag vs. Se.

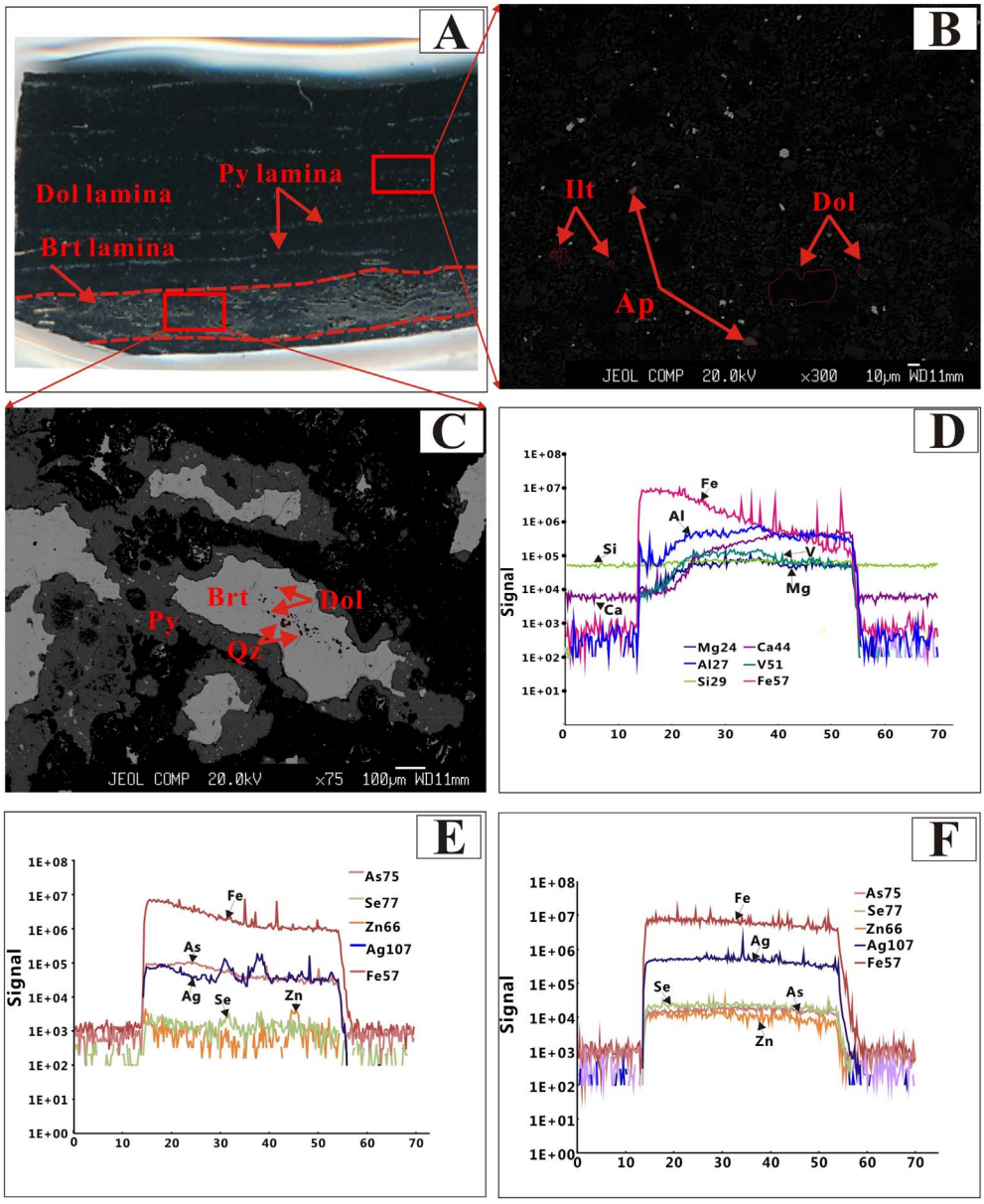

Fig. 6. BSE images of gangue minerals and LA-ICP-MS spectrum of different occurrences of pyrite from the Baiguoyuan Ag-V ore deposit, Hubei Province. A) Dolomite laminae interbedded by pyrite laminae and barite laminae (sample BGY-14b). B) Dolomite, illite and apatite disseminated within dolomite laminae. C) Dolomite and quartz included in barite. D) LA-ICP-MS spectrum indicating of V-bearing mineral inclusion and dolomite inclusion within Py2a. E) LA-ICP-MS spectrum indicating of Ag-bearing mineral inclusion and Ag solid solution within Py2a. F) LA-ICP-MS spectrum indicating of Ag solid solution in Py2a.
Py = pyrite, Brt = barite, Dol = dolomite, Ilt = illite, Ap = apatite, Qz = quartz.

deposit (Chen and Xie, 1986). The reason for the lack of those Ag minerals in this study remains an open question. Based on our results that the naumannite is very rare in amount, it can be inferred that naumannite is not the main mineral phase accounting for Ag in the ores.

Invisible Ag is detected in all occurrences of pyrite in this study. It is supposed that Ag occupies place of Fe and enters into lattice of pyrite (see Section 5.3 for more details). The negative correlation of Ag and Fe in pyrite supports this opinion (Fig. 5A). The lack of inclusions in the spectrum of LA-ICP-MS in Py2a and Py2b indicated presence of solid solution of Ag in pyrite (Fig. 6E, F). Taking account of the percentage of pyrite and their Ag contents, a preliminary mass balance calculation indicates that lattice Ag in pyrite may equal to 83 ppm Ag in the ores, which accounts for the main part of average Ag grade (116 ppm) of the Baiguoyuan Ag-V ore deposit. It, thus, can be proposed that the major Ag in the ores may be present as solid solution in pyrite.

5.3. Source of Ag

Naumannite has been reported only in several volcanic epithermal ore deposits, for example, the Broken Hills Pb-Zn-Ag ore deposit (Australian), the Rogovik Au-Ag ore deposit (Russia), the E'rentaolegai Ag ore deposit (China), and the northern Great Basin Au ore deposits (USA), where naumannite occurs as micron inclusions (1–10 μm) in pyrite (Kamenov et al., 2007; Cocker et al., 2013; Zhuravkova et al., 2015; Tian, 2015). The presence of naumannite in the Baiguoyuan Ag-V ore deposit would also indicate that Ag might source from volcanic activity. Considering no presence of contemporaneous volcanic rocks in the mining area, we suggest that the Ag-bearing hydrothermal fluid might be related to the submarine hydrothermal venting. The hydrothermal vent was recorded by sedimentary pyrite (Py2a and Py2b) as discussed below.

Concentrations and ratios of trace elements in pyrite may serve as good genetic indicators (Loftus-Hills and Solomon, 1967; Branov et al., 1972; Bralia et al., 1979; Mookherjee and Philip, 1979; Bajwah et al., 1987; Rao and Naqvi, 1997; Suurajit and Biswajit, 2011; Mustafa et al., 2014; Zhang et al., 2014a, 2014b). Generally, hydrogenic pyrite contains low Se (0.5–2 ppm) with S/Se ratios between 2.5×10^5 and 5.0×10^5, whereas hydrothermal pyrite contains high Se (20–50 ppm) with S/Se ratios between 1×10^4 and 2.67×10^4, and pyrite related to volcanism contains even higher Se with S/Se ratios in the order of

n × 10^3. In the Baiguoyuan Ag-V ore deposit, pyrite shows high concentrations of Se with average values of 174–1707 ppm, and the S/Se ratios vary between 4.37 × 10^2 and 2.21 × 10^3 (Fig. 5B). The Se contents and S/Se ratios in most pyrites are similar to those of volcanic-related pyrite. This indicates that there might be an input of volcanic hydrothermal fluid during formation of Py2a and Py2b. For Py3 and Py4, the relative higher Se contents and S/Se ratios may inherit from ambient material during diagenesis and post-diagenetic reworking.

The Co/Ni ratio has long been used to determine the origin of pyrite. Syngenetic/diagenetic pyrite always contains lower Co (< 1000 ppm) with Co/Ni ratios < 1.0, while hydrothermal pyrite contains higher Co (400–2400 ppm) with Co/Ni ratios > 1.0 (Large et al., 2009; Koglin et al., 2010; Reich et al., 2016). Most pyrite formed from lower temperature hydrothermal fluids has Co/Ni ratios between 10 and 5 and > 10 in volcanogenic pyrite (Bralia et al., 1979; Mookherjee and Philip, 1979). Bajwah et al. (1987) suggested that high Co/Ni ratios in pyrite are characteristics of mafic sources. For example, Co contents in pyrite from the Zijinshan volcanic hydrothermal Au-Cu ore deposit and from the Shagou hydrothermal vein-type Ag-Pb-Zn ore deposit are up to 1000 ppm with Co/Ni ratios > 1.0 (Li et al., 2010; Zhang et al., 2014b). In the Baiguoyuan Ag-V ore deposit, Co contents in pyrite vary from 733 ppm to 903 ppm, and their Co/Ni ratios are higher than 1.0 with except for only several pyrites (Fig. 5C). The exceptions could be due to high Ni in pyrite (up to 3090 ppm). Such high Ni and low Co/Ni ratios have been observed in pyrite that forms in organic matter-rich environments. And more reducing conditions have been found to enhance the uptake of Ni into pyrite (Large et al., 2014; Keith et al., 2016; Gregory et al., 2017). The Co contents and Co/Ni ratios in most pyrites are comparable to those of hydrothermal pyrite, indicating that the formation of those sedimentary-type Py2a and Py2b may relate to hydrothermal venting. For Py3 and Py4, the relative higher Co contents and Co/Ni ratios in them may inherit from ambient material during diagenesis and post-diagenetic reworking.

In summary, the lattice Ag in Py2a and Py2b may supply by hydrothermal venting which could be induced by submarine volcanism, and the lattice Ag in Py3 and Py4 may source from ambient material during diagenesis and post-diagenetic reworking.

5.4. Enrichment mechanism of Ag

Ag-bearing minerals are found in many ore deposits, such as the Howard's Pass Sedex Zn-Pb ore deposit (Canada), the Red Dog Sedex Zn-Pb-Ag ore deposit (USA), the Silvermines Pb-Zn-Ag ore deposit (Ireland), the Broken Hill Pb-Zn-Ag ore deposit (Australian), and the Pueblo Viejo epithermal ore deposit (Dominican Republic).

In the Howard's Pass Sedex Zn-Pb ore deposit, Ag was enriched in millimeter galena inclusions within pyrite (Gadd et al., 2016). In the Red Dog Sedex Zn-Pb-Ag ore deposit, Ag resided in galena, chalcopyrite and tetrahedrite inclusions within pyrite and sphalerite (Kelly et al., 2004). In the Silvermines Sedex ore deposit, Ag was enriched in sphalerite and tennantite (Lowell, 1985). In the Broken Hill Pb-Zn-Ag ore deposit, Ag was gathered in micron inclusions or other nearby minerals in pyrite (Cocker et al., 2013). In the VMS ore deposits in eastern Australia, high Ag concentrations were associated with inclusions of galena, tennantite and tetrahedrite (Huston et al., 1995). In the Pueblo Viejo epithermal Au-Ag ore deposit, high concentration of Ag is mostly due to the Pb sulfide nanoparticles within pyrite (Deditius et al., 2011). Almost all the deposits noted above pointed that the enrichment of Ag in pyrite was actually related to micron inclusions of Cu-Pb-Sn sulfide minerals. In this study, microscopy observation and BSE imaging found no inclusions of Cu-Pb-Sn sulfide minerals in pyrite, and EMPA data shows no enrichment of Pb-Cu-Sb in pyrite (Table 1), indicating that the enrichment mechanism of Ag in the Baiguoyuan Ag-V ore deposit was not related to inclusions of Cu-Pb-Sn sulfide minerals. Other mechanism is therefore needed.

The reason why pyrite crystal itself may not incorporate large amounts of Ag could be the difference of ionic radius and charge between Ag^+ and Fe^{2+} ion. The larger ionic radius of Ag^+ led to instability of complexation with S^- ion and hence limit substitution for Fe^{2+} in pyrite. As discovered in this study, Ag can combine with Se to form stable mineral, and the Se contents in pyrite are indeed very high. It was, thus, suggested that the high concentration of lattice Ag in pyrite (up to 6360 ppm) in the Baiguoyuan Ag-V ore deposit could be attributed to the high concentration of Se which may replace S during Ag incorporating into pyrite. This opinion is supported by the positive correlation between Ag and Se contents (Fig. 5D). Hence, we propose that the enrichment of Ag in pyrite can be achieved by the following pathways:

$$FeCl_2 + AgCl + H_2S + H_2Se \rightarrow (Fe, Ag)(S, Se)_2 + HCl \quad (1)$$

$$FeCl_2 + AgHS + H_2S + H_2Se \rightarrow (Fe, Ag)(S, Se)_2 + HCl \quad (2)$$

It is well known that Ag is soluble at high Cl concentrations in hydrothermal systems of lower pH (e.g., Seward, 1976; Gammons and Williams-Jones, 1995). It is also known that Ag-bisulfide complexing may exist in the ore-forming system according to the pH, i.e., AgHS(aq) is the dominant species in acidic solutions, $Ag(HS)_2^-$ under neutral pH conditions and $Ag_2S(HS)_2^{2-}$ in alkaline solutions (e.g., Gammons and Barnes, 1989; Renders and Seward, 1989; Stefansson and Seward, 2003).

Stefansson and Seward (2003) also indicated that the aqueous speciation of silver is very sensitive to fluid composition and temperature. Their experiment data suggested that below 100 °C silver(I) sulfide complexes predominate in reduced sulfide solutions, whereas Ag^+ and $AgClOH^-$ are the dominant species in oxidised waters. These authors also suggested that chloride complexes of silver (I) are most important in high-temperature hydrothermal solutions of seawater salinity. However, sulfide complexes may predominate in low-temperature geothermal systems, Due to the low temperature nature of the Baiguoyuan Ag-V ore deposit, the Ag-sulfide complexes may play a more important role during mineralization.

6. Conclusions

Based on studies of mineralography and pyrite chemistry in the black shale-hosted Baiguoyuan Ag-V ore deposit, Xingshan County, Hubei Province, the following conclusions can be drawn:

(1) Silver has two occurrences: micron naumannite inclusions and solid solution Ag in pyrite, and the latter one is the main occurrence which accounts for ca. 72% of the total Ag reserve.

(2) Silver was likely supplied by submarine hydrothermal venting during formation of sedimentary pyrite (Py2a and Py2b), and was inherited from ambient material during formation of diagenetic and post-diagenetic pyrite (Py3 and Py4).

(3) Silver was enriched through a mechanism with Ag replacing Fe and Se replacing S in pyrite.

Supplementary data to this article can be found online at https://doi.org/10.1016/j.gexplo.2017.10.005.

Acknowledgments

This study is funded by National Science Foundation of China projects (41272037, 41230102), China Geological Survey project (12120113094200) and the MOST Special Fund from the State Key Laboratory of Geological Processes and Mineral Resources, China University of Geosciences (No. MSFGPMR03-2). We thank Dr. Yang Shuiyuan for his help with the EMPA analyses. We are also grateful to Profs. David Lentz, Raymond Coveney and two anonymous reviewers who provided valuable comments and suggestions which helped to improve this manuscript significantly.

References

Bajwah, Z.U., Seccombe, P.K., Offler, R., 1987. Trace element distribution, Co: Ni ratios and genesis of the Big Cadia iron-copper deposit, New South Wales, Australia. Mineral. Deposita 22, 292–300.

Bralia, A., Sabatini, G., Troja, F., 1979. A revaluation of the Co/Ni ratio in pyrite as geochemical tool in ore genesis problems. Mineral. Deposita 14, 353–374.

Branov, E.N., Zasukhin, G.N., Karpukhina, V.S., Loginova, L.A., Bukharova, V.A., 1972. Occurrence of Cu, Zn, Pb and other elements in pyrite from aureoles of pyrite deposits. Geochem. Int. 9, 834–844.

Cabri, L.J., 1992. The distribution of trace precious metals in minerals and mineral products. Mineral. Mag. 56, 289–308.

Chen, C., Xie, F.P., 1986. An account of the Baiguoyuan black shale type silver-vanadium deposit. Mineral Deposits 1, 53–62 (in Chinese with English abstract).

Chen, K.X., Yang, Z.Q., Jin, G.F., Xie, F.P., 1997. A preliminary discussion on silver enrichment mechanism in the diagenetic process of the Baiguoyuan silver-vanadium deposit, Hubei Province. Mineral Deposits 16, 54–55 (in Chinese with English abstract).

Cocker, H.A., Mauk, J.L., Rabone, S.D.C., 2013. The origin of Ag–Au–S–Se minerals in adularia-sericite epithermal deposits: constraints from the Broken Hills deposit, Hauraki Goldfield, New Zealand. Mineral. Deposita 48, 249–266.

Condon, D., Zhu, M.Y., Bowring, S., Wang, W., Yang, A.H., Jin, Y.G., 2005. U-Pb ages from the Neoproterozoic Doushantuo Formation, China. Science 308 (5718), 95–98.

Costagliola, P., Di Benedetto, F., Benvenuti, M., Bernardini, G.P., Cipriani, C., Lattanzi, P.F., Romanelli, M., 2003. Chemical speciation of Ag in galena by EPR spectroscopy. Am. Mineral. 88, 1345–1350.

Deditius, A.P., Utsunomiya, S., Reich, M., Kesler, S.E., Ewing, R.C., Hough, R., Walshe, J., 2011. Trace metal nanoparticles in pyrite. Ore Geol. Rev. 42, 32–46.

Gadd, M.G., Layton-Matthews, D., Peter, J.M., Paradis, S.J., 2016. The world-class Howard's pass SEDEX Zn-Pb district, Selwyn Basin, Yukon. Part I: trace element compositions of pyrite record input of hydrothermal, diagenetic, and metamorphic fluids to mineralization. Mineral. Deposita 51, 319–342.

Gammons, C.H., Barnes, H.L., 1989. The solubility of Ag_2S in near-neutral aqueous sulfide solutions at 25 to 300 °C. Geochim. Cosmochim. Acta 53 (2), 279–290.

Gregory, D.D., Large, R.R., Halpin, J.A., Baturina, E.L., Lyons, T.W., Wu, S., Danyushevsky, L., Sack, P.J., Chappaz, A., Maslennikov, V.V., 2015. Trace element content of sedimentary pyrite in black shales. Econ. Geol. 110, 1389–1410.

Gregory, D., Lyons, T.W., Large, R., Jiang, G., Stepanov, A.S., Diamond, C.W., Figueroa, M.C., Olin, P., 2017. Whole rock and discrete pyrite geochemistry as complementary tracers of ancient ocean chemistry: an example from the Neoproterozoic Doushantuo Formation, China. Geochim. Cosmochim. Acta 216, 201–220.

Gammons, C.H., Williams-Jones, A.E., 1995. The solubility of Au-Ag alloy + AgCl in HCl/NaCl solutions at 300 °C: new data on the stability of Au(I) chloride complexes in hydrothermal solutions. Geochim. Cosmochim. Acta 59, 3453–3468.

Hua, M.C., 1988. The facies control of the black shale type of Ag and V deposit in western Hubei. Hubei Geol. 2, 26–40 (in Chinese with English abstract).

Huston, D.L., Sie, S.H., Suter, G.F., Cooke, D.R., Both, R.A., 1995. Trace elements in sulfide minerals from eastern Australian volcanic-hosted massive sulfide deposits; part I, proton microprobe analyses of pyrite, chalcopyrite, and sphalerite, and part II, selenium levels in pyrite; comparison with delta ^{34}S values and implications for the source of sulfur in volcanogenic hydrothermal systems. Econ. Geol. 90, 1167–1196.

Jiang, G.Q., Shi, X.Y., Zhang, S.H., Wang, Y., Xiao, S.H., 2011. Stratigraphy and paleogeography of the Ediacaran Doushantuo Formation (ca. 635–551 Ma) in South China. Gondwana Res. 19, 831–849.

Kamenov, G.D., Saunders, J.A., Hames, W.E., Unger, D.L., 2007. Mafic magmas as sources for gold in middle Miocene epithermal deposits of the northern Great Basin, United States: evidence from Pb isotope compositions of native gold. Econ. Geol. 102, 1191–1195.

Keith, M., Haase, K.M., Klemd, R., Krumm, S., Strauss, H., 2016. Systematic variations of trace element and sulfur isotope compositions in pyrite with stratigraphic depth in the Skouriotissa volcanic-hosted massive sulfide deposit, Troodos ophiolite, Cyprus. Chem. Geol. 423, 7–18.

Kelly, K.D., Leach, D.L., Johnson, C.A., Clark, J.L., Fayek, M., Slack, J.F., Anderson, V.M., Ayuso, R.A., Ridley, W.I., 2004. Textural, compositional, and sulfur isotope variations of sulfide minerals in the red dog Zn-Pb-Ag deposits, Brooks Range, Alaska: implications for ore formation. Econ. Geol. 99, 1509–1532.

Koglin, N., Frimmel, H.E., Lawrie Minter, W.E., Brätz, H., 2010. Trace-element characteristics of different pyrite types in Mesoarchaean to Palaeoproterozoic placer deposits. Mineral. Deposita 45, 259–280.

Large, R.R., Danyushevsky, L., Hollit, C., Maslennikov, V., Meffre, S., Gilbert, S., Bull, S., Scott, R., Emsbo, P., Thomas, H., Singh, B., Foster, J., 2009. Gold and trace element zonation in pyrite using a laser imaging technique: implications for the timing of gold in orogenic and Carlin-style sediment-hosted deposits. Econ. Geol. 104, 635–668.

Large, R., Halpin, J.A., Danyushevsky, L.V., Maslennikov, V., Bull, S.W., Long, J.A., Gregory, D., Lounejeva, E., Lyons, Patrick, T.W., Sack, J., McGoldrick, P.J., Calver, C.R., 2014. Trace element content of sedimentary pyrite as a new proxy for deep-time ocean–atmosphere evolution. Earth Planet. Sci. Lett. 389, 209–220.

Li, Z.K., Li, J.W., Chen, L., 2010. Occurrence of silver in the Shagou Ag-Pb-Zn deposit, Luoning County, Henan Province: implication for mechanism of silver enrichment. Earth Sci. J. China Univ. Geosci. 35, 621–636 (in Chinese with English abstract).

Li, F.H., Yang, G.Z., Yao, Y., Liao, Z.M., Liu, S.D., He, H.T., Tian, D.C., 2014. Basic characteristics and metallogenic model of Baiguoyuan silver-vanadium deposit in Xingshan County,Hubei Province. Resour. Environ. Eng. 28, 246–252 (in Chinese with English abstract).

Liu, Y.J., Jin, G.F., Xie, F.P., 1996. Metallogenesis and environment of a large Ag-V deposit in the black rock series. Hubei Geol. 10, 22–37 (in Chinese with English abstract).

Liu, P.J., Yin, C.Y., Gao, L.Z., Tang, F., Chen, S.M., 2009. New material of microfossils from the Ediacaran Doushantuo Formation in the Zhangcunping area, Yichang, Hubei Province and its zircon SHRIMP U–Pb age. Chin. Sci. Bull. 54 (6), 1058–1064.

Loftus-Hills, G., Solomon, M., 1967. Cobalt, nickel and selenium in sulphides as indicators of ore genesis. Mineral. Deposita 2, 228–242.

Lowell, G.R., 1985. Silver-bearing inclusions in “Argentiferous” galena from the Silvermines district in Southeastern Missouri Claudia Gasparrini. Can. Mineral. 23, 99–102.

Lu, J.L., Zhuang, H.P., Fu, J.M., Jinzhing, L., 1999. Occurrence of Ag and V of Baibuoyuan black shale-hosted silver and vanadium deposit in Hubei Province, China. Geochimica 28, 222–230 (in Chinese with English abstract).

Mookherjee, A., Philip, R., 1979. Distribution of copper, cobalt and nickel in ores and host-rocks, Ingladhal, Karnataka, India. Mineral. Deposita 14, 33–55.

Mustafa, A., Nail, Y., Burcu, G., Esra, Y., Semiha, I., 2014. The origin of vein-type copper-lead-zinc deposits host in Palaeozoic metamorphic rocks at the Southeast Anatolian Orogenic Belt (Küplüce-Adıyaman, Southeastern Turkey). J. Afr. Earth Sci. 102, 191–202.

Rao, D.S., Naqvi, S.M., 1997. Geological setting, mineralogy, geochemistry and genesis of the Middle Archaean Kalyadi copper deposit, western Dharwar craton, southern India. Mineral. Deposita 32, 230–242.

Reich, M., Simon, A.C., Deditius, A., Barra, F., Chryssoulis, S., Lagas, G., Tardani, D., Knipping, J., Bilenker, L., Sanchez-Alfaro, P., Roberts, M.P., Munizaga, R., 2016. Trace element signature of pyrite from the Los Colorados iron oxide-apatite (IOA) deposit in Chile: a missing link between Andean IOA and iron oxide copper-gold systems? Econ. Geol. 111, 743–761.

Renders, P.J., Seward, T.M., 1989. The stability of hydrosulphido- and sulphido-complexes of Au(I) and Ag(I) at 25 °C. Geochim. Cosmochim. Acta 53 (2), 245–253.

Seward, T.M., 1976. The stability of chloride complexes of silver in hydrothermal solutions up to 350 °C. Geochim. Cosmochim. Acta 40, 1329–1341.

Sharp, T., Buseck, P.R., 1993. The distribution of Ag and Sb in galena. Am. Mineral. 78, 85–95.

Stefansson, A., Seward, T.M., 2003. Experimental determination of the stability and stoichiometry of sulphide complexes of silver(I) in hydrothermal solutions to 400 °C. Geochim. Cosmochim. Acta 67 (7), 1395–1413.

Suurajit, S., Biswajit, M., 2011. Chemical and sulphur isotope compositions of pyrite in the Jaduguda U (–Cu–Fe) deposit, Singhbhum shear zone, eastern India: Implications for sulphide mineralization. J. Earth Syst. Sci. 120, 475–488.

Tian, J., 2015. Mineralization and alteration geological characteristics study in E`rentaolegai silver deposit. In: Inner Mongolia: [Dissertation]. China University of Geosciences (Beijing), China (in Chinese).

Yang, Z.Q., Chen, K.X., Jin, G.F., Xie, F.P., 1996. Evidence for the Late Proterozoic catastrophic events in Xingshan County: microspherules and negative anomalies of carbon isotopes. Reg. Geol. China 1, 83–87 (in Chinese with English abstract).

Yang, B., Hu, B., Bao, Z., Zhang, Z., 2011. REE geochemical characteristics and depositional environment of the black shale-hosted Baiguoyuan Ag-V deposit in Xingshan, Hubei Province, China. J. Rare Earths 29, 499–506.

Zhang, R.X., Yang, S.Y., 2016. A mathematical model for determining carbon coating thickness and its application in electron probe microanalysis. Microsc. Microanal. 22, 1374–1380.

Zhang, Q., Dong, Z.S., Zhan, X.Z., 1995. The geochemical characteristics of black shale type Ag-V deposit in Baiguoyuan. Acta Mineral. Sin. 15, 185–191 (in Chinese with English abstract).

Zhang, J., Deng, J., Chen, H.Y., Yang, L.Q., Cooke, D., Danyushevsky, L., Gong, Q.J., 2014a. LA-ICP-MS trace element analysis of pyrite from the Chang'an gold deposit, Sanjiang region, China: Implication for ore-forming process. Gondwana Res. 26, 557–575.

Zhang, W.Y., Wang, G.Z., Sun, Y.C., 2014b. Characteristics of zonal pyrite in Zijinshan Cu-Au deposit. Nonferrous Met. 66, 36–42 (in Chinese with English abstract).

Zhu, B., Becker, H., Jiang, S.-Y., Pi, D.-H., Fischer-Gödde, M., Yang, J.-H., 2013a. Re–Os geochronology of black shales from the Neoproterozoic Doushantuo Formation, Yangtze platform, South China. Precambrian Res. 225, 67–76.

Zhu, M., Lu, M., Zhang, J., Zhao, F., Li, G., Yang, A.H., Zhao, X., Zhao, M., 2013b. Carbon isotope chemostratigraphy and sedimentary facies evolution of the Ediacaran Doushantuo Formation in western Hubei, South China. Precambrian Res. 225, 7–28.

Zhuang, H., Lu, J., Fu, J., 1999. Evidence for transforming mineralization of Baiguoyuan silver-vanadium deposit hosted in black shale in Hubei, China. Chin. Sci. Bull. 44 (3), 263–267.

Zhuravkova, T.V., Palyanova, G.A., Kravtsova, R.G., 2015. Physicochemical formation conditions of silver sulfoselenides at the Rogovik deposit, Northeastern Russia. Geol. Ore Deposits 57, 313–330.